Research Article Vol. 14, No. 11 / 1 Nov 2023 / Biomedical Optics Express 5555
Biomedical Optics EXPRESS

Ratiometric fluorescence sensing and quantification of circulating blood sodium sensors in mice *in vivo*

FERNANDO IVICH, ISEN CALDERON, QIANQIAN FANG, HEATHER CLARK, AND MARK NIEDRE*

Department of Bioengineering, Northeastern University, Boston, MA 02120, USA
**m.niedre@neu.edu*

Abstract: In this work, we introduce ratiometric diffuse *in vivo* flow cytometry (R-DiFC) for quantitative measurement of circulating fluorescent red blood cell (fRBC) sensors for systemic blood sodium levels. Unlike in our previous work in measuring circulating fRBC sensors, R-DiFC allows simultaneous measurement of two fluorophores encapsulated in the sensor, the ratio of which enables self-calibration of the fluorescence signal with different fRBC depths in biological tissue. We show that the R-DiFC signal varies significantly less than either fluorescence signal alone. This work holds promise for personalized monitoring of systemic sodium for bipolar patients in the future.

1. Introduction

Diffuse *in vivo* Flow Cytometry (DiFC) is an optical technique that uses highly-scattered light to detect and count fluorescently-labeled cells or circulating sensors flowing in deep-seated blood vessels in mice without having to draw blood [1,2]. Transient fluorescent peaks are detected as labeled cells move through a blood vessel in the DiFC field-of-view. Compared to intra-vital microscopy methods of *in vivo* circulating cell detection, use of diffuse photons in DiFC allows sampling of larger, deeply seated blood vessels. This allows us to sample larger circulating blood volumes and enumerate comparably rare circulating cells. To date, we have primarily used DiFC to detect circulating tumor cells in mouse models of cancer metastasis [3–6].

Recently, we used DiFC to detect circulating fluorescent sensors, termed "fluorescent Red Blood Cells" (fRBCs) [2], which are micron-sized erythrocyte membrane-camouflaged sensors that were developed for continuous monitoring of systemic blood sodium levels. A major long-term motivation of fRBC technology is to create a personalized drug dose monitoring method for bipolar disorder patients treated with lithium. Briefly, bipolar disorder is a serious psychiatric disease that affects millions of people in the United States and the world [7,8]. The gold standard treatment is still lithium [9] which unfortunately has a narrow therapeutic drug dose range (0.6-1.2 mM) that is very close to levels (>1.5 mM) [10] at which serious toxicity and kidney damage may occur [11], specifically, a decrease in sodium reabsorption. Normal blood sodium levels range between 135 mM and 145 mM. Extreme cases of hyponatremia and hypernatremia are in the range of ~100 mM [12] and ~225 mM [13], respectively, the former being a potential side effect of lithium that can induce seizures and death. Because of this, some patients under lithium treatment have blood samples drawn weekly to measure sodium levels, but this precludes measurement of more rapid fluctuations in sodium levels over the timespan of hours or days [14,15]. Most experimental methods for measuring sodium also rely on drawing blood samples and subsequent analysis with spectroscopic or electrochemical methods [16]. The vision of our fRBC technology is to allow continuous *in vivo* monitoring of sodium levels using an external optical reader. This would preclude the need for blood draws and could enable more frequent treatment monitoring and mitigation of harmful side effects.

#499263 https://doi.org/10.1364/BOE.499263
Journal © 2023 Received 30 Jun 2023; revised 22 Sep 2023; accepted 22 Sep 2023; published 3 Oct 2023

Biomedical Optics EXPRESS

In our prior work, we used DiFC to monitor the circulation lifetime of fRBCs *in vivo* using red fluorescence (640 nm excitation, 680 nm emission) [2]. We showed that the use of erythrocyte coatings extended the circulation lifetime (half-life) compared to PEG coated sensors. However, one of the major challenges in quantifying red fluorescence signals *in vivo* with DiFC was the effect of fRBC sensor depth on the measured fluorescence intensity at the surface. Because DiFC operates in the diffusive photon propagation regime, the signal was influenced by both the optical scattering and attenuation in tissue. As a result, the fluorescence signal varied significantly with only hundreds of micrometer changes in depth [17].

In this manuscript, we introduce "Ratiometric DiFC (R-DiFC)". The concept is to decrease the fRBC fluorescence signal variability at different depths by using green (Rhodamine 18) fluorescence as a reference self-calibration signal for the red (Chromoionophore III) fluorescence [18]. To do this, we designed and built a new DiFC system to measure both fluorescence signals simultaneously. We show that this ratio decreases with increasing sodium concentration as expected and varies significantly less with sensor depth than either fluorophore alone.

2. Materials and methods

2.1. Ratiometric diffuse in vivo flow cytometer

Figure 1 shows a schematic diagram (Fig. 1(a)) and photograph (Fig. 1(b)) of the R-DiFC instrument. Our R-DiFC instrument uses two continuous wave diode-pumped solid state laser sources to fluorescently excite the fRBC sensors: a 640 nm (CL-640-100, CrystaLaser LLC, Reno, NV), and a 555 nm (CL-555-100, CrystaLaser). A free-space optical isolator (IO-5-560-HP, Thorlabs Inc, Newton, NJ) placed in front of the 555 nm laser prevents back reflections into the green laser cavity and improves stability. The output of each laser is passed through a cleanup bandpass (BP-x) filter (640/20-25 and 554/23-25, Semrock, West Henrietta, NY), and then through a neutral density (ND) filter. A dichroic filter (Di-x; FF605-DI02, Semrock) oriented at 45 degrees combines the red and green lasers into a single beam. A second dichroic (Di; FF650/659-Di01-25 × 36, Semrock) directs the beam into a long working distance, infinity-corrected 2x objective (#59-875, Edmund Optics Inc, Barrington, NJ), which focuses the light onto a 1 mm spot at the sample. The power at the sample is 20 mW for both lasers.

The emitted fluorescence light is collected through the objective and passed through two notch filters (ZET561NF and ZET635NF, Chroma Technology Corporation, Bellows Falls, VT) to remove any residual contribution from the lasers in the fluorescence detection channels. A third dichroic (Di-m; T660lpxrxt, Chroma) further splits the emitted light into the two channels, which are then passed through bandpass filters (BP-m; 585/40 nm and 680/42 nm, Semrock). Fluorescence light for each channel is focused with two 25 mm-diameter plano-convex lenses (45-363, Edmund) and detected with two photomultiplier tubes (PMTs; H10721-29, Hamamatsu Photonics, Bridgewater, NJ). The output of the PMTs is amplified and filtered (100 Hz short pass) with low-noise preamplifiers (PA; SR560, Stanford Research Systems, Sunnyvale, CA). Finally, the signal is digitized using an analog-to-digital converter (DAQ; USB-6212, National Instruments, Austin, TX) with a sampling rate of 2 kHz.

2.2. R-DiFC data analysis

The data analysis workflow used for R-DiFC data is shown schematically in Fig. 2. The data was processed using methodology building on our previously reported work [1,3,5] as follows. Step (iii) below is unique to R-DIFC:

i) Pre-processing: We first subtracted the non-specific autofluorescence background from the raw data for each fluorescence channel. The background was estimated by applying a 5-second moving median filter to each, which was then subtracted from the original signal.

Biomedical Optics EXPRESS

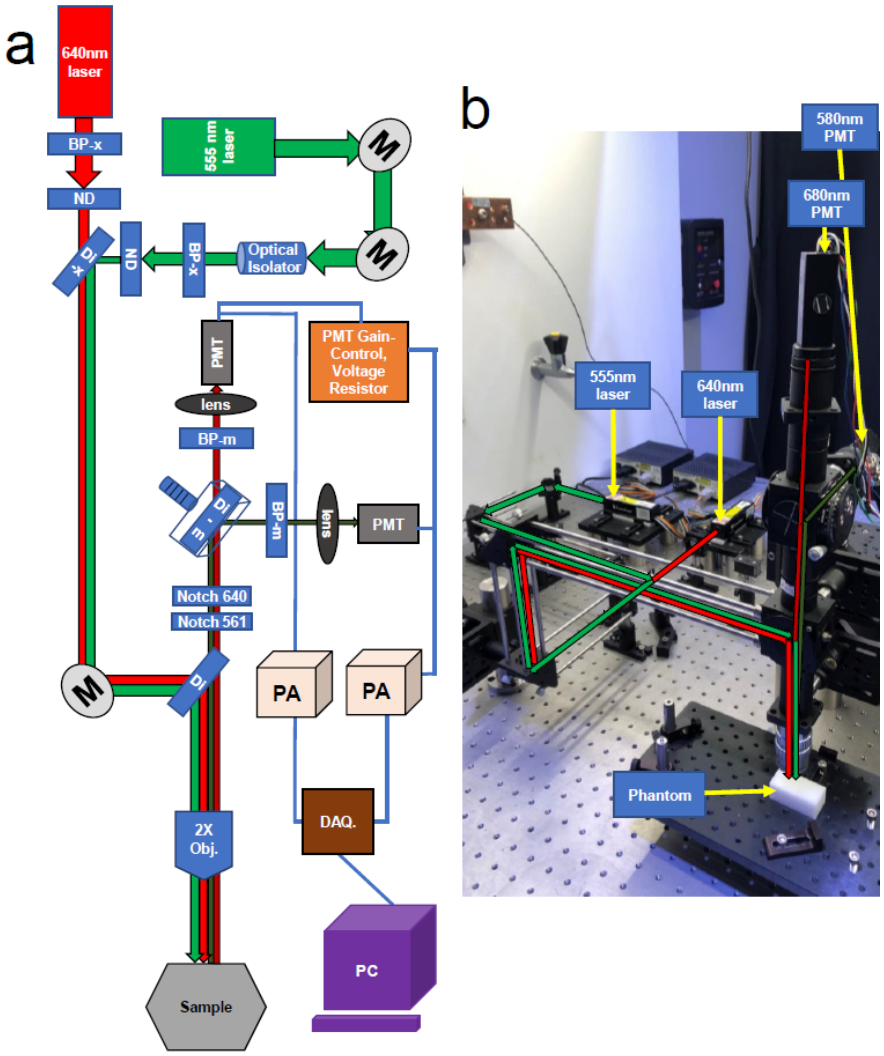

Fig. 1. R-DiFC (a) schematic diagram and (b) photograph. Red and green arrows show the light path from source to sample to detector. Abbreviations: BP, bandpass; ND, neutral density; Di, dichroic; M, mirror; Obj., objective; PMT, photomultiplier tube; PA, preamplifier, DAQ., data acquisition board; PC, personal computer. Subscripts: m, emission; x, excitation.

Biomedical Optics EXPRESS

We also applied a 10 ms smooth filter. We then calculated the standard deviation of the background-subtracted data in a 1-minute moving window for each channel.

ii) Peak identification: When a fluorescent microsphere or fRBC sensor passed through the R-DiFC field-of-view, transient fluorescence peaks are generated and detected. We identify these as peaks exceeding a threshold equal to five times the moving standard deviation as calculated above [19].

iii) Simultaneous detection and ratio calculation: Because fRBCs contain both green and red fluorophores (see section 2.3 below), we imposed a simultaneous detection condition, whereby a peak must be detected on both channels simultaneously inside a 0.03 s time window. This window size was determined heuristically by analysis of measured temporal peak full-width-half-maximum widths in our prior DiFC work, which are on the order of 0.01 s [1]. In the rare case of two peaks on a single channel (doublets) inside the 0.03 s window, the larger peak (amplitude) was used. The ratio of red-to-green fluorescence peak amplitudes was calculated for each coincident occurrence. Unmatched peaks were discarded from the analysis. As we discuss in the results section below, this generally occurred due to low detected peak amplitudes from the green channel due to attenuation of light in tissue. The mean of these ratios (on a peak-by-peak basis) for all detected fRBCs during the scan is then computed. Scans ranged from 5 minutes in phantoms to 25 minutes in mice.

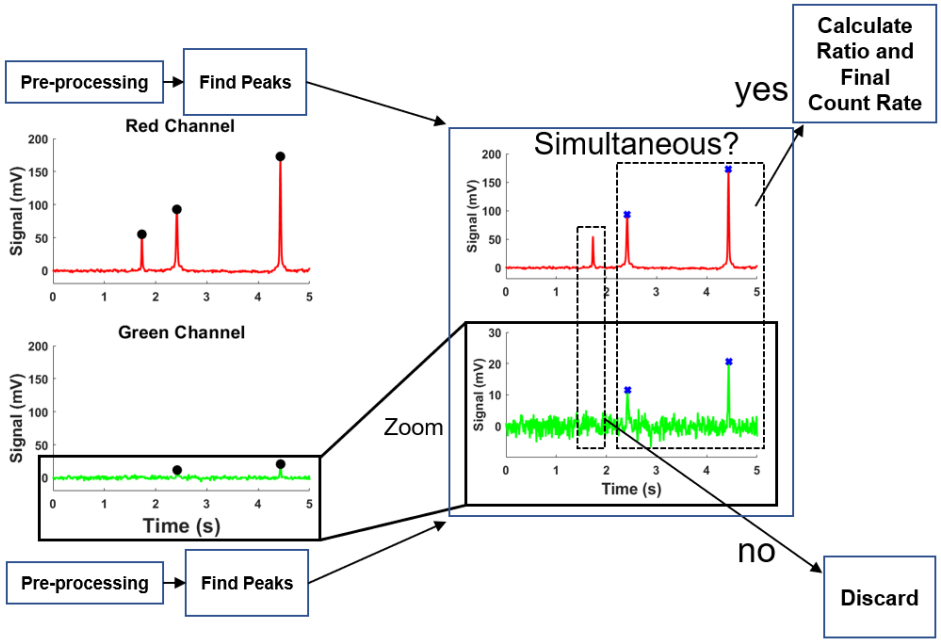

Fig. 2. R-DiFC data analysis workflow.

2.3. *Fluorescent red blood cell (fRBC) sodium sensors*

The fRBCs used in this study were described in detail by our team previously [2]. Briefly, a polymer-free lipophilic plasticizer matrix acts as the sensor core where sensing components (i.e., sodium ionophore X, chromoionophore III, rhodamine 18, and ion exchanger NaTFPB) are

Biomedical Optics EXPRESS

dissolved. Red blood cell (RBC) membranes were prepared from rat blood (Sprague Dawley, Innovative Research Inc., Novi, MI). 100 µL of the optode cocktail was dispersed and emulsified with the RBC membrane through vigorous mixing for 5 min (vortex). The suspension was then washed with 10 mM HEPES solution (pH 7.4) to remove excess cell debris.

Figure 3 shows a schematic diagram of an fRBC and its interaction with sodium. The optically inactive sodium ionophore X extracts Na^+ ions from the external environment (blood) into the lipophilic sensor core. To maintain charge neutrality within the sensor core, H^+ ions are exchanged into the external environment, resulting in a change of the local pH within the sensor core (Fig. 3(a)). The local pH in the sensor core increases as sodium concentration increases, decreasing the fluorescence intensity of chromoionophore III (red) and slightly increasing the intensity of the reference fluorophore rhodamine 18 (green) [20]. Figure 3(b) shows the fRBC ratiometric response to varying $[Na^+]$ (N = 3 repeats) measured with a commercial fluorescence plate reader (Spectramax M3, Molecular Devices, San Jose, CA). As shown, the signal ratio decreased with increasing $[Na^+]$. The physiologically relevant systemic $[Na^+]$ levels are indicated with vertical lines. We also show (inset) an expanded view of the physiological range for clarity. The entire sensor core is encapsulated with an RBC membrane which, as we showed previously, increased the circulation lifetime of the fRBCs compared to PEGylated coatings [2].

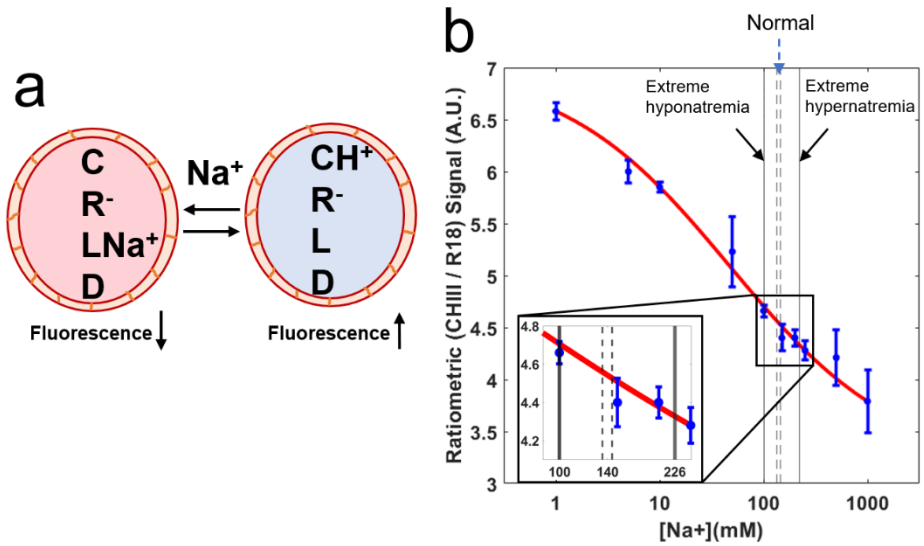

Fig. 3. (a) Schematic diagram of circulating fRBCs, which alter their fluorescence signal in the presence of $[Na^+]$; C, chromoionophore III; R-, ion exchanger NaTFPB; L, sodium ionophore; D, Rhodamine 18. (b) The ratio of red (CHIII) and green (R18) fluorescence signals measured with a fluorescence plate reader in the presence of increasing $[Na^+]$, showing the response of fRBCs. Blue data points and error bars represent averages and ranges, respectively, from N = 3 repeats. The vertical solid and dashed lines indicate clinically relevant blood $[Na^+]$ in humans.

2.4. *Optical phantom models in vitro*

As an initial test of R-DiFC, we used a tissue-mimicking optical flow phantom that approximates the optical properties of biological tissue as we have done previously [19]. The phantom is made of high-density polyethylene and has holes drilled at different depths where we thread microbore Tygon tubing (TGY-010-C, Small Parts, Inc., Seattle, WA). The tubing is connected to a syringe

Biomedical Optics EXPRESS

pump (70-2209, Harvard Apparatus, Holliston, MA) that flows fluorescent microspheres or fRBC sensors through the phantom block.

We used Envy Green fluorescent microspheres (FSEG008, Bangs Laboratories Inc., Fisher, IN) and Flash Red reference intensity 5 fluorescent microspheres (FR5; Bangs). Fluorescent microspheres were suspended at a concentration of 10^3 per mL in phosphate buffer saline (PBS) to prevent doublet counting and pumped at a flow rate of 50 µL per minute for 5 minutes (N = 5 repeats) to approximate *in vivo* flow rate linear velocities of a mouse tail artery [5,21]. We also used PBS solution with no microspheres as a control to determine the system's false alarm rate.

We also used suspensions of fRBC sensors in HEPES solutions with known Na^+ concentrations (1, 5, 10, 50, 100, 150, 200, 250, 500, and 1000 mM) at 0.75 mm and 1 mm depth in the phantom model (N = 3 repeats).

2.5. Mouse experiments

In vivo mouse studies were conducted in accordance with Northeastern University's Institutional Animal Care and Use Committee (IACUC) policies of animal care, protocol #20-1037R. We used 7–8-week-old athymic nude mice under a low-fluorescence chow diet. During R-DiFC scanning, we anesthetized the animals with 2% isoflurane and regulated their temperature with heating pads. We injected one hundred thousand fRBCs suspended in 100 µL of HEPES solution into circulation using an insulin syringe needle through retro-orbital injection and scanned the middle of the tail (aligned above the ventral caudal artery) of the mice for 25 minutes. After scanning, we drew 100 µL blood samples and measured sodium levels independently using a commercial blood analyzer, i-STAT loaded with EC8 + cartridges (Abbott Laboratories, Chicago, IL).

2.6. Monte Carlo simulations of photon transport and diffuse fluorescence signal modeling

A major consideration of using fluorescence amplitude to quantify sodium concentration is the effect of sensor depth in the tissue on the measurement, i.e., due to the attenuation of light as it propagates through biological tissues. We modeled R-DiFC using Monte Carlo (MC) simulations of photon propagation in 3-dimensional diffusive media using Monte Carlo eXtreme (MCX) software [22,23]. We computed the sensitivity matrix (Jacobian) using the adjoint method for a source-detector separation of 0 mm using representative optical properties for red and green wavelengths from the literature [17]. Specifically, for the red wavelength, we used scattering and absorption coefficients of $\mu_s = 10\,\mathrm{mm}^{-1}$ and $\mu_a = 0.025\,\mathrm{mm}^{-1}$. As we discuss in more detail in section 3.2, we used a range of optical properties for green wavelengths, specifically μ_s from 12.5 to 25 mm^{-1} and μ_a from 0.03 to 0.05 mm^{-1}. The index of refraction, n, and the anisotropy coefficient, g, were set to 1.37 and 0.9, respectively in all cases. We used an isotropic $5 \times 5 \times 5$ cm^3 volume with a voxel size of $250 \times 250 \times 250$ $\mu\mathrm{m}^3$ to simulate 10^8 photon packets over a time gate of 5 ns.

Similar to our previously published analysis of DiFC signals in tissue [19], we used MC simulations to calculate the theoretical R-DiFC signal from different fRBC depths in tissue. To do this, we used the first Born approximation denoted by the following equation [24]

$$\Phi_{fl}(r_d, r_s) = W^{fl}(r_j; r_s, r_d)\, \eta_{fl}(r_j),$$

where $W^{fl}(r_j; r_s, r_d)$ denotes the Jacobian matrix, computed using the adjoint method [25] and the output of the simulations above; $\eta_{fl}(r_j)$ is the fluorophore concentration associated with a small fluorescence perturbation, in this case the fluorescence signal as a function of position in the medium. $\Phi_{fl}(r_d, r_s)$ is the fluorescence signal measured between a source and detector located at r_s and r_d, respectively. To estimate η, we used experimental DiFC measurements of fRBCs at a depth of 0.75 mm in a phantom (measured separately for green and red fluorophores). We then used the obtained values of η to estimate the theoretical ratiometric signal, $\Phi_{fl}(r_d, r_s)$, at

Biomedical Optics EXPRESS

different depths ranging from 0.75 to 2 mm, approximately matching the expected depths for blood vessels in a mouse tail (as we do here) or for a superficial blood vessel in the wrist of a human, which may range from 2 to 4 mm [26].

3. Results

3.1. Validation of R-DiFC with fluorescent microspheres in flow phantoms in vitro

We first tested R-DiFC with suspensions of Envy Green and FR5 microspheres in a flow phantom *in vitro* as shown in Fig. 4. A photograph of the phantom irradiated by red and green laser light with embedded tubing attached to a syringe and connected to the pump is presented in Fig. 4(a). Sample data sets of detected peaks are shown, labeled with black circles. Each peak represents detection of the fluorescence signal from a single microsphere passing through the R-DiFC field-of-view. Figures 4(b-d) show sample data when microspheres were run through tubes embedded 0.75 mm deep in a phantom. Figure 4(b) shows sample R-DiFC data from a suspension of Envy Green microspheres only, demonstrating negligible fluorophore "bleed" into the red channel. Likewise, Fig. 4(c) shows sample results measured from a suspension of only FR5 microspheres, again demonstrating no fluorescence bleed into the green channel. Note that the absolute noise is similar on the red and green channels (~2 mV), however the relative noise is higher on the green channel due to the lower amplitude peaks. Finally, Fig. 4(d) shows data from mixed suspensions of both Envy Green and FR5 microspheres. These data demonstrate that the R-DiFC enables measurement of both green and red fluorescence signals independently with negligible bleed between channels.

3.2. Ratiometric fluorescence measurements have less depth dependance than single fluorescence measurements

Figure 5 shows both the Monte Carlo simulated and measured (phantoms) reduction in peak amplitude for red (Fig. 5(a)), and green (Fig. 5(b)) diffuse fluorescence signals. Results from Monte Carlo light models (solid lines) are shown, indicating a decrease in fluorescence intensity of 99.3% and 99.2% for red and green signals for fRBC depths increasing from 0.75 to 2 mm. Experimental DiFC measurements from fRBCs in phantoms are also shown (symbols, N = 3 repeats). These agree well with the MC, showing a significant decrease of red (CHIII) and green (R18) fluorescence in Figs. 5(a) and (b), respectively. This illustrates the challenge of quantifying sodium (or other analyte) concentrations from measuring absolute fluorescence intensities in biological tissue *in vivo*. Figure 5(c) shows the normalized theoretical and experimental ratio of red:green fluorescence signals, with an average predicted ratiometric signal variation of only 24.5% from 0.75 mm to 2 mm deep. To test the sensitivity of this result to the assumed optical properties of the phantom block, we varied the coefficients of scattering (μ_s) and absorption (μ_a) for the green signal (in the MC simulations) from 12.5 mm^{-1} to 25 mm^{-1} and from 0.03 mm^{-1} to 0.05 mm^{-1}, respectively. As shown, the predicted ratiometric signal stays relatively invariant with tissue depth.

3.3. Validation of fluorescent red blood cell sensors in flow phantoms in vitro

Next, we tested R-DiFC using the fRBC microsensors with varying concentrations of Na^+ in flow phantoms *in vitro* [2]. Representative data is shown in Fig. 6. We used suspensions of fRBCs at 1 mm depth with [Na^+] ranging from 1 mM (Fig. 6(a)) to 1000 mM (Fig. 6(b)). As shown, the detected fluorescence signal amplitude for the red peaks was significantly reduced in the presence of higher [Na^+] (Fig. 6(a) versus Fig. 6(b)). For this experiment, the mean peak amplitude (of ~200 detected peaks) of the red fluorescence signal reduced from 189.3 ± 77.8 mV to 65.8 ± 16.4 mV. To illustrate this, the average and range of the red fluorescence of the fRBCs in response to increasing [Na^+] (as in our previous work [2]) is shown in Fig. 6(c). A sigmoidal

Biomedical Optics EXPRESS

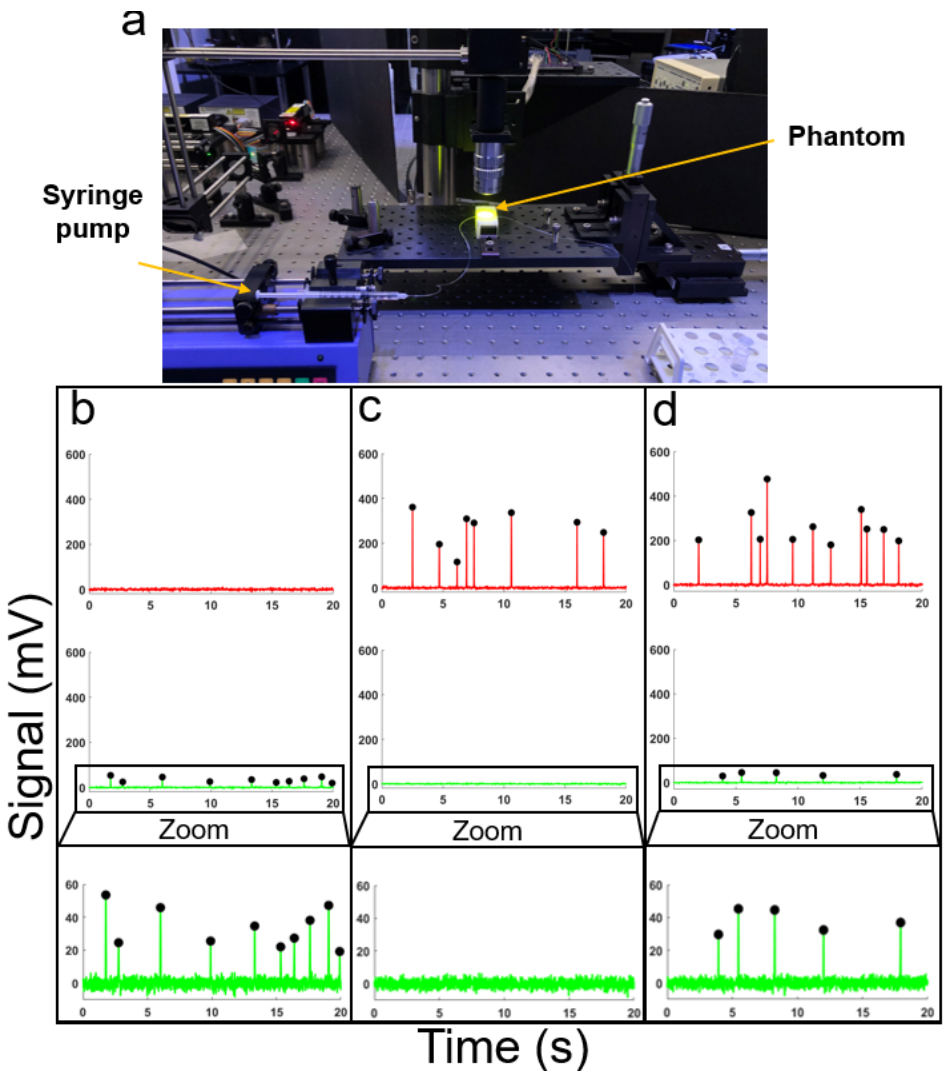

Fig. 4. (a) R-DiFC measurements from fluorescent microspheres flowing through a tissue mimicking phantom. We tested (b) Envy Green microspheres only,(c) FR5 microspheres only, and (d) mixed suspensions of Envy Green and FR5 microspheres.

Biomedical Optics EXPRESS

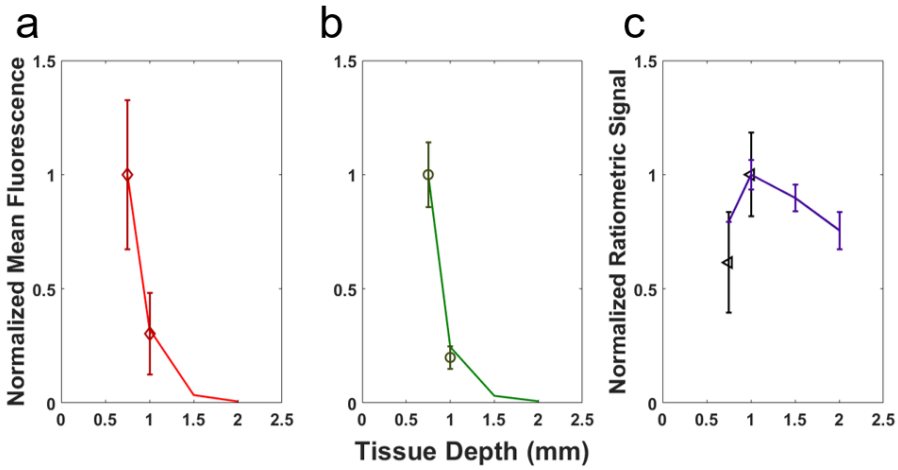

Fig. 5. Monte Carlo derived (solid line) and experimental (symbols) red, green and red:green ratiometric signals as a function of depth. Normalized mean peak amplitude for (a) red (640 nm) fluorescence (CHIII) and (b) green (555 nm) fluorescence (R18) wavelengths. (c) Normalized ratiometric signal between red and green signals. The error bars in the simulation results on (c) indicate a range of assumed optical properties.

curve fit is shown in red. The green fluorescence signal is not shown since it was unchanged on average from 18.0 ± 4.5 mV to 18.7 ± 8.1 mV.

The ratiometric data are summarized in Fig. 6(d), which shows the red:green fluorescence signal as a function of [Na^+]. Only peaks where simultaneous detections on both the red and green channels (corresponding to a single detected fRBC) were included in the ratio calculations. The peakwise average ratio of red and green amplitudes (blue data points) with their corresponding signal range (error bars) from N = 3 repeats are shown. The ratiometric signal decreased from 10.2 ± 1.9 to 3.7 ± 0.8 (mV/mV) as [Na^+] increased from 1 to 1000 mM. The effect of the peakwise self-calibration of the red-to-green fluorescence signals is to decrease the observed range bars which can originate from depth-attenuation effects, as well as differences in sensor size (fluorophore concentration). A sigmoidal curve fit to the data is also shown. The vertical dashed and solid lines indicate the respective normal and hypo/hypernatremia [Na^+] that are observed clinically [12,13]. The response sensitivity of R-DiFC to fRBCs over this physiological range was 15.3%. In comparison, using red fluorescence (Fig. 6(c)) the response sensitivity over the physiological range was 12.2%. However, the error bars with red fluorescence were significantly larger than ratiometric measurements (6.5-fold) from 100 to 250 mM [Na^+], which shows the advantage of using a reference signal for self-calibration.

3.4. *Testing of R-DiFC in mice in vivo*

Figure 7 summarizes proof-of-concept testing of R-DiFC in mice *in vivo*. We scanned the ventral side of the tail of nude mice injected with fRBCs as shown in Fig. 7(a) (note that the combined red and green light produce a yellow color). Examples of detected red and green fluorescence data measured are shown in Fig. 7(b). Simultaneous (matched) peaks from fRBCs are labeled with a blue 'x'. We also noted an increase in unmatched peaks due to fewer detections in the green channel relative to the phantom measurements. We attribute this to increased attenuation of green fluorescence light through biological tissue. The mean and range of the ratios on a peak-by-peak basis from N = 3 mice are indicated as the open green circle in Fig. 7(c). The mouse's systemic sodium concentration was also measured independently with a commercial

Biomedical Optics EXPRESS

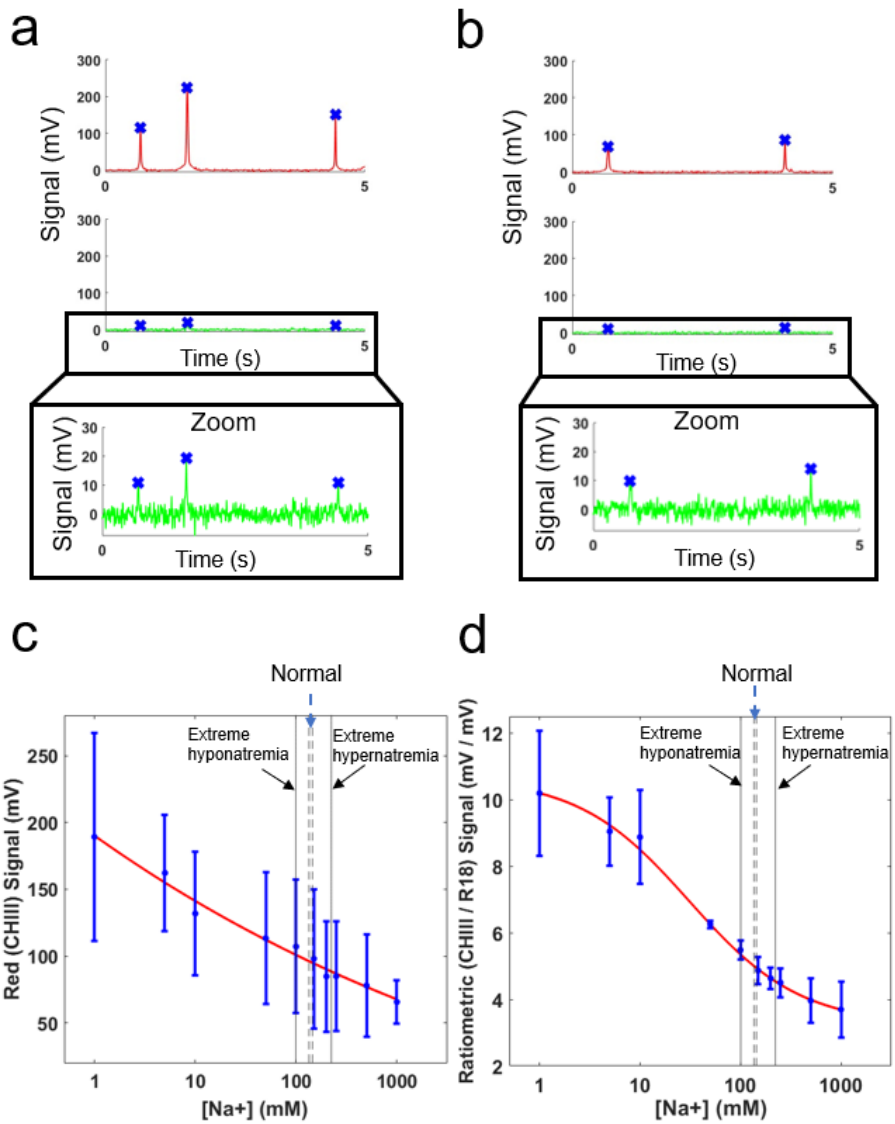

Fig. 6. R-DiFC measurements of fRBCs in phantoms *in vitro*. Example R-DiFC data of fRBCs with (a) 1 mM and (b) 1000 mM [Na^+] *in vitro*. The fRBC average and range (error bars) of (c) red fluorescence only (as in [2]), and (d) ratiometric red:green signals measured in phantoms over the range of [Na^+] is shown (blue points with red sigmoidal fit). Solid and dashed vertical lines indicate clinically relevant range of blood sodium concentrations.

Biomedical Optics EXPRESS

blood analyzer and averaged over the three mice, yielding the actual [Na^+] value of 133.7 ± 5.5 mM. Note that the x-axis range bar is smaller than the symbol. We included in Fig. 7(c) the R-DiFC-fRBC [Na^+] calibration curve measured from our flow phantom experiments (Fig. 6(d)) in blue.

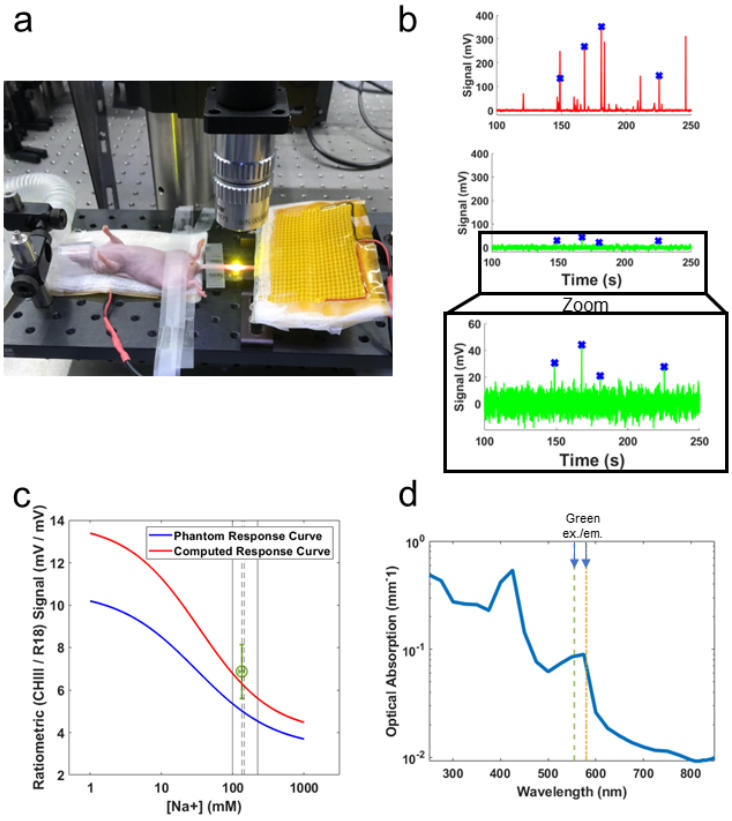

Fig. 7. R-DiFC measurements of circulating fRBC sensors in mice *in vivo*. (a) Photograph of a mouse during R-DiFC scanning. (b) Representative red and green fluorescence data collected from mice *in vivo*. Coincident detected peaks are labeled with blue crosses. The average ratio and range across (N = 3) mice tested is shown in (c) with a green circle. The ratiometric response curve measured from the flow phantom (blue solid line) and recalculated with higher absorption at green wavelengths (red solid line) as would be expected *in vivo*. Vertical lines represent ranges of physiological human blood sodium concentrations. (d) Representative absorption coefficient (mm^{-1}) of biological tissue is shown [17] along with the excitation and emission wavelengths, respectively, of the green fluorophore R18.

We expect that the optical absorption in a mouse tail is higher than that in the phantom due to the presence of a local hemoglobin absorption peak in the spectral region of the R18 fluorophore as shown in Fig. 7(d) [17]. As such, we also re-computed the sodium response curve using an MC simulation with higher optical absorption ($\mu_a = 0.1\ mm^{-1}$) for the green signal, which is shown in red in Fig. 7(c). As would be expected, the increased absorption of green light reduced the green fluorescence signal at the surface and therefore shifted the ratiometric signal up. The resulting curve is in good agreement with the experimental data collected in mice. In summary, proof-of-concept R-DiFC measurements *in vivo* generally agree with the expected signal range based on our phantom data and expected optical properties in biological tissue. Future strategies for improving this agreement are discussed in more detail below.

Biomedical Optics EXPRESS

4. Discussion and conclusions

We previously used red fluorescence DiFC and circulating fRBCs to measure sodium ion concentration in mouse blood *in vivo* using a single red fluorophore and laser source [2]. The purpose of this work was to introduce R-DiFC that allowed measurement of red and green fluorescence signals from fRBCs simultaneously, with the aim of improving the accuracy of quantitative fluorescence measurements with varying tissue depth [27].

Unlike our previously reported DiFC systems which used optical fiber-based designs [1,3,5], R-DiFC uses a free beam design (Fig. 1). This optical configuration enabled simultaneous illumination with two laser wavelengths and detection of two fluorophores, which is currently infeasible with our fiber-based approach. We also implemented a coincidence (matching) algorithm (Fig. 2) to detect fluorescent events simultaneously in both red and green channels and compute the ratio on a peak-by-peak basis.

As we showed both computationally and experimentally (Fig. 5), the ratiometric signal is significantly less sensitive to depth-attenuation effects than either fluorophore alone. Specifically, the ratiometric signal only varies by approximately 25% over the first 2 mm of tissue depth, whereas a single wavelength signal decreases more than 99%. We showed that this effect was consistent across a range of phantom-approximated *in vivo* optical properties [17,28].

We also demonstrated that we could perform R-DiFC measurements from circulating fRBCs in mice *in vivo*. In this proof-of-concept study, the ratiometric signal generally agreed with the expected signal range given the high attenuation of green light *in vivo* (Figs. 7(b) and (c)). In principle it would also be possible to shift the excitation wavelength to slightly longer wavelengths for the R18 fluorophore to mitigate this, however in this study we were limited by hardware constraints (laser and filter) in our instrument. In addition, based on the R18 absorption spectrum the maximum achievable shift would be only about 15 nm. Although the measured ratio is relatively insensitive to the depth of the fRBC, we expect that the fRBC ratiometric response curve (Fig. 6(d)) will shift in the presence of different tissue optical properties (Fig. 7(c)). Therefore, any future use in humans would require an accurate response curve for individual patients. In principle this could be achieved by measurement of tissue optical properties and recalculation of the dose response curve using Monte Carlo models as we have done here. In addition, we plan to shift the wavelength of the reference fluorophore to a longer wavelength to reduce light attenuation *in vivo* and increase the amplitude and number of fRBC detections.

In principle, translating DiFC to humans could be achieved by scanning a major blood vessel such as the radial artery in the wrist. Since this blood vessel carries ~100 mL of blood per minute [29,30], this would enable scanning of about 1 L of peripheral blood volume in 10 minutes [31]. Given that accurate estimation of sodium concentration requires at least 10^3 fRBC detections, we would require on the order of 1 fRBC in circulation per mL of peripheral blood in steady state to achieve an estimate in a 10-minute scan. In mice (given the ~100 µL per minute flow rate in a mouse tail), the needed concentration would be approximately three orders of magnitude higher. With respect to laser safety, the maximum permissible skin exposure set by the Electrotechnical Commission (IEC) limits 200 mW/cm^2 for visible light and 300 mW/cm^2 for near infrared light [32]. With 20 mW illumination, this could be achieved by increasing the illumination spot size in the range of 3-4 mm in diameter. We showed previously that this would have negligible impact on signal detection at the blood vessel depth [19]. The fRBC platform could also be expanded and adapted for other types of blood analytes in the future.

Funding. National Institute of Biomedical Imaging and Bioengineering (1R01EB024186-01A1).

Disclosures. The authors have no conflicts of interests, financial or otherwise, to disclose.

Data Availability. Matlab code for the Monte Carlo simulations, the processing of experimental data and the generation of the figures can be found in Github open-source library [33]. Raw Matlab data files with the Jacobians and the fRBC and microsphere data can be found in Pennsieve data sharing platform repository [34].

Biomedical Optics EXPRESS

References

1. X. Tan, R. Patil, P. Bartosik, J. M. Runnels, C. P. Lin, and M. Niedre, "In Vivo Flow Cytometry of Extremely Rare Circulating Cells," Sci. Rep. **9**(1), 3366 (2019).
2. W. Di, X. Tan, I. A. C. Calderon, A. E. Neal Reilly, M. Niedre, and H. A. Clark, "Real-time particle-by-particle detection of erythrocyte-camouflaged microsensor with extended circulation time in the bloodstream," Proc. Natl. Acad. Sci. U.S.A. **117**(7), 3509–3517 (2020).
3. J. Pace, F. Ivich, E. Marple, and M. Niedre, "Near-infrared diffuse in vivo flow cytometry," J. Biomed. Opt. **27**(09), 097002 (2022).
4. A. L. Williams, J. E. Fitzgerald, F. Ivich, E. D. Sontag, and M. Niedre, "Short-Term Circulating Tumor Cell Dynamics in Mouse Xenograft Models and Implications for Liquid Biopsy," Front. Oncol. **10**, 601085 (2020).
5. R. Patil, X. Tan, P. Bartosik, A. Detappe, J. M. Runnels, I. Ghobrial, C. P. Lin, and M. Niedre, "Fluorescence monitoring of rare circulating tumor cell and cluster dissemination in a multiple myeloma xenograft model in vivo," J. Biomed. Opt. **24**(08), 1 (2019).
6. J. E. Fitzgerald, B. K. Byrd, R. A. Patil, R. R. Strawbridge, S. C. Davis, C. Bellini, and M. Niedre, "Heterogeneity of circulating tumor cell dissemination and lung metastases in a subcutaneous Lewis lung carcinoma model," Biomed. Opt. Express **11**(7), 3633–3647 (2020).
7. X. Pérez de Mendiola, D. Hidalgo-Mazzei, E. Vieta, and A. González-Pinto, "Overview of lithium's use: a nationwide survey," Int. J. Bipolar Disord. **9**(1), 10 (2021).
8. R. Machado-Vieira, H. K. Manji, and C. A. Zarate, "The role of lithium in the treatment of bipolar disorder: convergent evidence for neurotrophic effects as a unifying hypothesis," Bipolar Disord. **11**(s2), 92–109 (2009).
9. R. H. Lenox and R. L. Papke, "Neurobiology of Lithium: An Update," J Clin Psychiatry 11 (n.d.).
10. R. T. Timmer and J. M. Sands, "Lithium Intoxication," JASN **10**(3), 666–674 (1999).
11. W. M. Bennett, "Drug interactions and consequences of sodium restriction," Am. J. Clin. Nutr. **65**(2), 678S–681S (1997).
12. N. Zhou and C. Yang, "A case of extreme hyponatremia without neurologic symptoms," Clin. Case Rep. **7**(10), 1874–1879 (2019).
13. M. H. Arambewela, N. P. Somasundaram, and C. Garusinghe, "Extreme hypernatremia as a probable cause of fatal arrhythmia: a case report," J. Med. Case Rep. **10**(1), 272 (2016).
14. Mark. E. Meyerhoff, "In vivo blood-gas and electrolyte sensors: Progress and challenges," TrAC Trends Anal. Chem. **12**(6), 257–266 (1993).
15. N. J. Schork, "Personalized medicine: Time for one-person trials," Nature **520**(7549), 609–611 (2015).
16. M. Sheikh, M. Qassem, I. F. Triantis, and P. A. Kyriacou, "Advances in Therapeutic Monitoring of Lithium in the Management of Bipolar Disorder," Sensors **22**(3), 736 (2022).
17. S. L. Jacques, "Optical properties of biological tissues: a review," Phys. Med. Biol. **58**(11), R37–R61 (2013).
18. M. R. Herling and I. J. Dmochowski, "Ratiometric, pH-Sensitive Probe for Monitoring siRNA Delivery," J. Am. Chem. Soc. **145**(17), 9417–9422 (2023).
19. F. Ivich, J. Pace, A. L. Williams, M. Shumel, Q. Fang, and M. Niedre, "Signal and measurement considerations for human translation of diffuse in vivo flow cytometry," J. Biomed. Opt. **27**(06), 067001 (2022).
20. T. T. Ruckh, A. A. Mehta, J. M. Dubach, and H. A. Clark, "Polymer-Free Optode Nanosensors for Dynamic, Reversible and Ratiometric Sodium Imaging in the Physiological Range," Sci. Rep. **3**(1), 3366 (2013).
21. E. Zettergren, D. Vickers, J. Runnels, S. K. Murthy, C. P. Lin, and M. Niedre, "Instrument for fluorescence sensing of circulating cells with diffuse light in mice in vivo," J. Biomed. Opt. **17**(3), 037001 (2012).
22. Q. Fang and D. A. Boas, "Monte Carlo Simulation of Photon Migration in 3D Turbid Media Accelerated by Graphics Processing Units," Opt. Express **17**(22), 20178 (2009).
23. L. Yu, F. Nina-Paravecino, D. Kaeli, and Q. Fang, "Scalable and massively parallel Monte Carlo photon transport simulations for heterogeneous computing platforms," J. Biomed. Opt. **23**(01), 1 (2018).
24. S. R. Arridge and J. C. Schotland, "Optical tomography: forward and inverse problems," Inverse Probl. **25**(12), 123010 (2009).
25. Q. Fang, S. A. Carp, J. Selb, G. Boverman, Q. Zhang, D. B. Kopans, R. H. Moore, E. L. Miller, D. H. Brooks, and D. A. Boas, "Combined Optical Imaging and Mammography of the Healthy Breast: Optical Contrast Derived From Breast Structure and Compression," IEEE Trans. Med. Imaging **28**(1), 30–42 (2009).
26. Z. Domagała, J. Grzelak, N. Pospiech, N. Hunter, J. Klekowski, A. Lach, K. Stój, B. Kurc-Darak, and M. Trzaska, "Ultrasound evaluation of the radial artery in young adults — A pilot study," Ann. Anatomy - Anatomischer Anzeiger **238**, 151763 (2021).
27. X. Huang, J. Song, B. C. Yung, X. Huang, Y. Xiong, and X. Chen, "Ratiometric optical nanoprobes enable accurate molecular detection and imaging," Chem. Soc. Rev. **47**(8), 2873–2920 (2018).
28. S. Brooks, C. L. Hoy, A. Amelink, D. J. Robinson, and T. E. Nijsten, "Sources of variability in the quantification of tissue optical properties by multidiameter single-fiber reflectance and fluorescence spectroscopy," J. Biomed. Opt. **20**(5), 057002 (2015).
29. L. J. Goldstein and S. Gupta, "Use of the Radial Artery for Hemodialysis Access," Arch. Surg. **138**(10), 1130–1134 (2003).
30. A. Masengu, J. McDaid, A. P. Maxwell, and J. B. Hanko, "Preoperative radial artery volume flow is predictive of arteriovenous fistula outcomes," J. Vascular Surg. **63**(2), 429–435 (2016).

Biomedical Optics EXPRESS

31. M. Niedre, "Prospects for Fluorescence Molecular In Vivo Liquid Biopsy of Circulating Tumor Cells in Humans," Front. Photonics **3**, 910035 (2022).
32. International Electrotechnical Commission, "Safety of laser products - Part 1: Equipment classification and requirements," (2014).
33. M. Niedre, "Ratiometric fluorescence sensing and quantification of circulating blood sodium sensors in mice *in vivo*: code," Github, 2023, https://github.com/mark-niedre/Ratiometric-DiFC.
34. F. Ivich and M. Niedre, "Ratiometric fluorescence sensing and quantification of circulating blood sodium sensors in mice *in vivo*: data," Pennsieve Discover, 2023, https://doi.org/10.26275/Q8WB-A9QE.